Imaging dispersive energy by slant stacking

Jianghai Xia, Kansas Geological Survey, The University of Kansas; Yixian Xu, China University of Geosciences; and Richard D. Miller, Kansas Geological Survey, The University of Kansas*

Summary

We present a new algorithm of calculating an image of dispersive energy in the frequency-velocity (*f*-*v*) domain. The frequency decomposition (Coruh, 1985) is first applied to a shot gather in the offset-time domain to stretch impulsive data into pseudo-vibroseis data or frequency-swept data. Because there is a deterministic relationship between frequency and time with a sweep that is used in the frequency decomposition, the first step theoretically completes the transform from time to frequency. The slant stacking is then performed on the frequency-swept data to complete the transform from offset to velocity. This simple two-step algorithm generates an image of dispersive energy in the *f*-*v* domain. The straightforward transform only uses offset information of data so that this algorithm can be applied to data acquired with arbitrary geophone-acquisition geometry. This algorithm breaks new ground for true 3D surface-wave analysis. Examples of synthetic and real-world data demonstrate that this algorithm generates accurate images of dispersive energy of the fundamental mode as well as higher modes.

Introduction

Multichannel analysis of surface waves—MASW (Park et al., 1999; Xia et al., 1999) utilizes a multichannel recording system to estimate near-surface shear (S)-wave velocity from high-frequency (≥ 2 Hz) Rayleigh waves. The method has been getting more and more attention from the near-surface geophysical community and has been applied to problems of near-surface geology and geophysics (e.g., Xia et al., 2002a, 2002b, 2002c, 2003, 2004; Miller et al., 1999; Beaty et al., 2002; Beaty and Schmitt, 2003; Tian et al., 2003a, 2003b; Lin and Chang, 2004; Yilmaz and Eser, 2002). One of the key steps of the MASW method is to generate an image of dispersion energy in the frequency-velocity (*f*-*v*) domain. Three algorithms are commonly used in high-frequency surface-wave analysis: the *F*-*K* transformation (e.g., Yilmaz, 1987), the Tau-p transform (McMechan and Yedlin, 1981), and the phase shift (Park et al., 1998). For the *F*-*K* transformation method, data in the *x*-*t* domain are first transformed into the *F*-*K* domain and then determination of phase velocities can be completed through the relation $v = f/k$, where v, f, and k are phase velocity, frequency, and wavenumber, respectively. Normally the *F*-*K* transformation results in an image of dispersion energy with poor resolution. In the Tau-p transform method, an image of dispersion energy is obtained by two phases of transforms. Data are first transformed into the Tau-p domain and a Fourier transform is then performed along the time. With the phase-shift method, a phase shift is applied to data according to an adopted velocity and a sum is then performed for each considered frequency. After evaluating these algorithms, Moro et al. (2003) concluded that the phase shift approach is not sensitive to data processing and maintains very good performances even with a limited number of traces; when fundamental mode detection is the primary concern and high-frequency overtones can be neglected, the phase shift method is a robust and cost-effective solution capable of providing accurate phase velocities.

Three methods, discussed previously, require data acquired along a straight line with evenly spaced receivers. In this paper, we develop an algorithm that can be applied to data acquired with receivers in an arbitrary acquisition geometry. The algorithm consists of two steps: data are first stretched into pseudo-vibroseis data or frequency-swept data and then the slant stacking is performed on the frequency-swept data. This two-step transform generates an image of dispersive energy in the *f*-*v* domain.

The algorithm

Assuming multichannel impulsive data $x(d, t)$ acquired in the *d*-*t* domain, where d is an offset (distance between a source and a receiver), the frequency decomposition (Coruh, 1985) is first applied to $x(d, t)$ that stretches $x(d, t)$ into pseudo-vibroseis data or frequency-swept data $X(d, t)$ by the following equation:

$$X(d, t) = S(t) \otimes x(d, t), \tag{1}$$

where $\otimes$ stands for the convolution operation, and $S(t)$ is a linear or non-linear sweep and should cover a frequency range of interest. Goupillaud (1976) provided a general form of $S(t)$: $S(t) = \mathrm{Im}\left\{\exp\left[i2\pi \int_0^t f(t)dt\right]\right\}$, where $f(t)$ is the instantaneous frequency and defines the relationship between time and frequency. After the frequency decomposition (Equation 1), therefore, we equivalently complete a transform from time to frequency. This decomposition can be omitted if vibroseis data are acquired.

The slant stack is applied to $X(d, t)$ with a predetermined velocity range that covers phase velocities of interest. Discussion of construction of slant stacks can be found in Yilmaz (1987, p. 430). We only list a couple equations used in our calculations. We first applied a linear moveout (LMO) correction to $X(d, t)$ through a coordinate transformation (Claerbout, 1978):

$$\tau = t - d/v. \quad (2)$$

After LMO, an event with slope $1/v$ on $X(d, t)$ is flat. Next, we summed the data over the offset axis to obtain

$$X(v, \tau) = \sum_d X\left(d, \tau + d/v\right). \quad (3)$$

By repeating the LMO (Equation 2) for values $v \in (v_{min}, v_{max})$ and stacking the data (Equation 3), we obtain an image in the t-v domain. As mentioned earlier, we can assign a specific time with a corresponding frequency depending on a sweep used in the frequency decomposition. Because we are interested in energy peaks, to generate a smoothed image of dispersive energy the maximum value of $X(v, \tau)$ in a time window (wl) is used to be assigned with a corresponding frequency. The length of the window wl could be selected in a wide range with little effect on the image as examples shown in the paper. In our testing, wl was selected corresponding to a frequency increment from 0.1 Hz to 2.0 Hz depending on a frequency range of the image. After assigning corresponding frequencies, we get the image of surface wave energy $X(f, v)$ in the f-v domain. Phase velocities of surface waves can then be picked up to form the fundamental and higher modes.

A synthetic example

High-frequency Rayleigh waves (Figure 1a) due to a two-layer model were simulated by a finite-difference method (Xu et al., in review). The model consists of the surface layer V_p = 800 m/s, V_s = 200 m/s, ρ = 2000 kg/m^3, and thickness = 10 m, and the half-space V_p = 1200 m/s, V_s = 400 m/s, and ρ = 2000 kg/m^3. Dispersive energy of Rayleigh waves was clearly shown in a synthetic shot gather with 60 channels (Figure 1a). The nearest offset of the shot gather is 1 m and receivers are 1 m apart. A 20-sec-long linear-up sweep from 2 Hz to 50 Hz was used to perform the frequency decomposition of the data (Figure 1a) with Equation 1. Figure 1b shows the first 8 s of frequency-swept data. The frequency-swept data (Figure 1b) were summed by slant stacking with a velocity range from 100 m/s to 700 m/s and an increment of 5 m/s. wl was selected as 0.2 s that corresponds to ~0.5 Hz. After assigning slant-stacked data with corresponding frequencies, we obtained the image in the f-v domain (Figure 1c).

Rayleigh-wave energy is dominant in the image (Figure 1c). We can pick phase velocities following higher peaks associated with energy trends. At some frequencies, for example, 25 Hz and 40 Hz, there is more than one peak due to higher modes. Asymptotes at the high and low frequencies of the fundamental mode (Figure 1c) indicate the correct phase velocities for the top layer (~190 m/s) and the half space (~370 m/s). The image also shows strong energy of the first, second, and third higher modes and provides sufficient resolution to distinguish these modes. Asymptotes of the higher modes approach to correct phase velocities, too. Asymptotes of higher modes at the high and low frequencies reach the S-wave velocities of the top layer and the half space, respectively. These characteristics are not the same as those of the fundamental mode.

The analytical results (solid dots, Figure 1c) calculated by the Knopoff method (Schwab and Knopoff, 1972) were used to check the accuracy of the image. For the fundamental mode, the image indicates a relatively low phase velocity (< 5%) at frequencies around 10 Hz and in the high frequencies range (> 40 Hz). For the first higher model, the image suggests a little high-phase velocity (< 5%) at frequencies around 25 Hz. Possible reasons could be near-field effects (e.g., non-plane wave propagation and body-wave energies) and finite-difference approximation (Xu et al., in review).

Real-world examples

Surface-wave data (Figure 2a) were acquired in Virginia Key, Florida, using a 24-channel seismograph with 14-Hz vertical-component geophones that were deployed at 0.6-m intervals with the nearest offset of 4.5 m (Xia et al., in review). The source was a 3.5-kg hammer vertically impacting a 0.3-m by 0.3-m metal plate. A 10-sec-long linear-up sweep from 10 Hz to 110 Hz was used to perform the frequency decomposition. The frequency-swept data were summed by the slant stacking with a velocity range from 20 m/s to 700 m/s and an increment of 5 m/s. wl was selected as 0.1 s that corresponds to ~1 Hz. After assigning slant-stacked data with corresponding frequencies, we obtained the image in the f-v domain (Figure 2b). We can pick phase velocities following higher peaks of energy trends (Figure 2b). Phase velocities with the fundamental mode can be determined from 20 Hz up to 100 Hz. Phase velocities of the first higher mode can also be picked up from 50 Hz to 90 Hz with no difficulty.

Data of the second real-world example (Figure 3a) were acquired in Olathe, Kansas, using a 60-channel seismograph with 4.5-Hz vertical-component geophones that were deployed at a 0.6-m interval with the nearest offset of 6.0 m (Miller et al., 1999). The source was a 5.4-kg hammer vertically impacting a 0.3-m by 0.3-m metal plate. A 10-sec-long linear-up sweep from 10 Hz to 110 Hz was used to perform the frequency decomposition. The slant stacking with a velocity range from 20 m/s to 700 m/s and an increment of 5 m/s was performed to the frequency-swept data. wl was selected as 0.2 s that corresponds to ~2 Hz. After assigning slant-stacked data with corresponding frequencies, we obtained the image in the f-v domain (Figure 3b). The

fundamental mode of a surface-wave energy trend was very well defined from 25 Hz to 80 Hz. We can easily pick phase velocities following higher peaks associated with the trend.

Discussion and Conclusions

The algorithm developed in the paper was applied to synthetic and real-world data along a straight line with evenly spaced receivers. The accuracy of the algorithm was assessed with synthetic data and analytic results. Synthetic and real-world examples demonstrated its ability to generate clear fundamental-mode as well as higher-mode images. As we mentioned in the paper, the length of time window (*wl*) is not critical to the quality of the image of dispersive energy so that it can be selected in a wide range. The real power of the algorithm is its capability to generate an image of dispersive energy from data acquired in an arbitrary acquisition geometry, which lays down a foundation for true 3D surface-wave analysis. Testing on 3D data will be our future task.

Acknowledgments

The authors are very grateful to Ronald Kaufmann and Richard Benson of Technos, Inc. for acquiring data used in the paper. The authors thank Marla Adkins-Heljeson of the Kansas Geological Survey for editing the manuscript.

References

Beaty, K.S., Schmitt, D.R., and Sacchi, M., 2002, Simulated annealing inversion of multimode Rayleigh wave dispersion curves for geological structure: Geophys. J. Int., 151**,** 622–631.

Beaty, K.S., and Schmitt, D.R., 2003, Repeatability of multimode Rayleigh-wave dispersion studies: Geophysics, 68, 782-790.

Claerbout, J.F., 1978, Snell waves: Stanford Exploration Project Report No. 15, 57-72, Stanford University.

Coruh, C., 1985, Stretched automatic amplitude adjustment of seismic data: Geophysics, 50, 252-256.

Goupillaud, P., 1976, Signal design in the "VIBROSEIS" technique: Geophysics, 41, 1291-1304.

Lin, C.-P., and Chang, T.-S., 2004, Multi-station analysis of surface wave dispersion: Soil Dynamics and Earthquake Engineering, 24(11), 877-886.

McMechan, G.A., and Yedlin, M.J., 1981, Analysis of dispersive waves by wave field transformation: Geophysics, 46, 869-874.

Miller, R.D., Xia, J., Park, C.B., and Ivanov, J., 1999, Multichannel analysis of surface waves to map bedrock: The Leading Edge, 18, 1392-1396.

Moro, G.D., Pipan, M., Forte, E., and Finetti, I., 2003*,* Determination of Rayleigh wave dispersion curves for near surface applications in unconsolidated sediments: Technical Program with Biographies, SEG, 73rd Annual Meeting, Dallas, TX, 1247-1250.

Park, C.B., Miller, R.D., and Xia, J., 1998, Imaging dispersion curves of surface waves on multi-channel record: Technical Program with Biographies, SEG, 68th Annual Meeting, New Orleans, Louisiana, 1377-1380.

Park, C.B., Miller, R.D., and Xia, J., 1999, Multichannel analysis of surface waves: Geophysics, 64, 800-808.

Schwab, F. A., and Knopoff, L., 1972, Fast surface wave and free mode computations: *in* Methods in Computational Physics, edited by B.A. Bolt: Academic Press, New York, 87-180.

Tian, G., Steeples, D.W., Xia, J., and Spikes, K.T., 2003a, Useful resorting in surface wave method with the autojuggie: Geophysics*,* 68, 1906-1908.

Tian, G., Steeples, D.W., Xia, J., Miller, R.D., Spikes, K.T., and Ralston, M.D., 2003b, Multichannel analysis of surface wave method with the autojuggie: Soil Dynamics and Earthquake Engineering, 23(3), 243-247.

Xia, J., Miller, R.D., and Park, C.B., 1999, Estimation of near-surface shear-wave velocity by inversion of Rayleigh wave: Geophysics, 64, 691-700.

Xia, J., Miller, R.D., Park, C.B., and Tian, G., 2002a, Determining Q of near-surface materials from Rayleigh waves: Journal of Applied Geophysics, 51(2-4), 121-129.

Xia, J., Miller, R.D., Park, C.B., Hunter, J.A., Harris, J.B., and Ivanov, J., 2002b, Comparing shear-wave velocity profiles from multichannel analysis of surface wave with borehole measurements: Soil Dynamics and Earthquake Engineering, 22(3), 181-190.

Xia, J., Miller, R.D., Park, C.B., Wightman, E., and Nigbor, R., 2002c, A pitfall in shallow shear-wave refraction surveying: Journal of Applied Geophysics, 51(1), 1-9.

Xia, J., Miller, R.D., Park, C.B., and Tian, G., 2003, Inversion of high frequency surface waves with fundamental and higher modes: Journal of Applied Geophysics, 52(1), 45-57.

Xia, J., Chen, C., Li, P.H., and Lewis, M.J., 2004, Delineation of a collapse feature in a noisy environment using a multichannel surface wave technique: Geotechnique, 54(1), 17-27.

Xia, J., Xu, Y., Chen, C., and Kaufmann, R.D., in review, Discussion on some practical equations with implications to high-frequency surface-wave techniques: Soil Dynamics and Earthquake Engineering.

Xu, Y., Xia, J., and Miller, R.D., in review, Finite-difference modeling of high-frequency Rayleigh-wave propagation for near-surface applications: Geophysical Journal International.

Yilmaz, Ö., 1987, Seismic data processing: Society of Exploration Geophysicists, Tulsa, OK.

Yilmaz, Ö., and Eser, M., 2002, A unified workflow for engineering seismology: Technical Program with Biographies, SEG, 72nd Annual Meeting, Salt Lake City, UT, 1496-1499.

Imaging dispersive energy by slant stacking

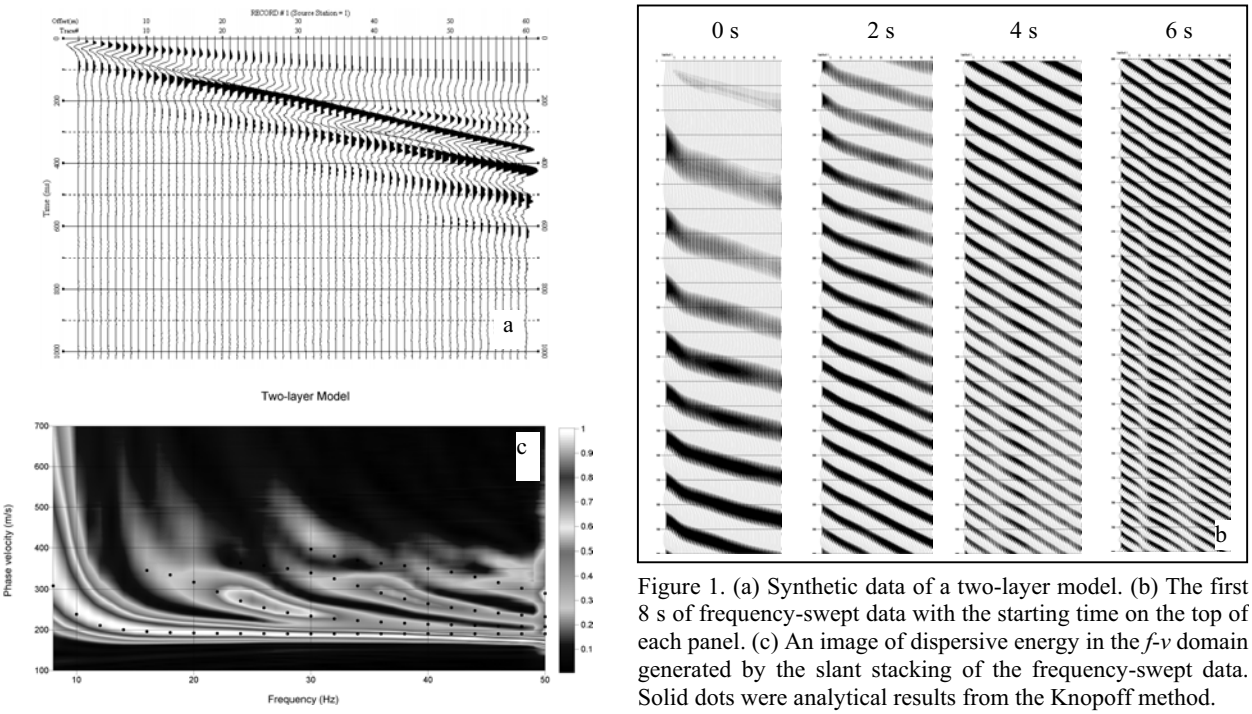

Figure 1. (a) Synthetic data of a two-layer model. (b) The first 8 s of frequency-swept data with the starting time on the top of each panel. (c) An image of dispersive energy in the *f-v* domain generated by the slant stacking of the frequency-swept data. Solid dots were analytical results from the Knopoff method.

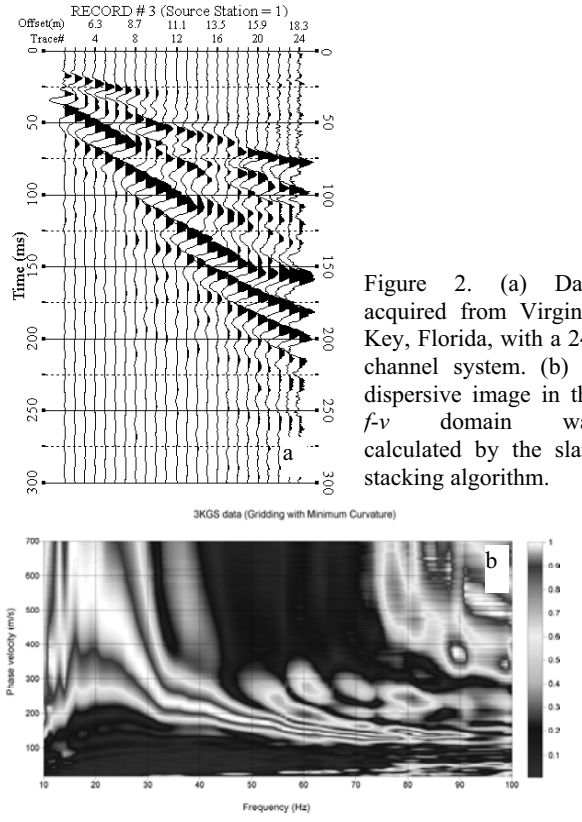

Figure 2. (a) Data acquired from Virginia Key, Florida, with a 24-channel system. (b) A dispersive image in the *f-v* domain was calculated by the slant stacking algorithm.

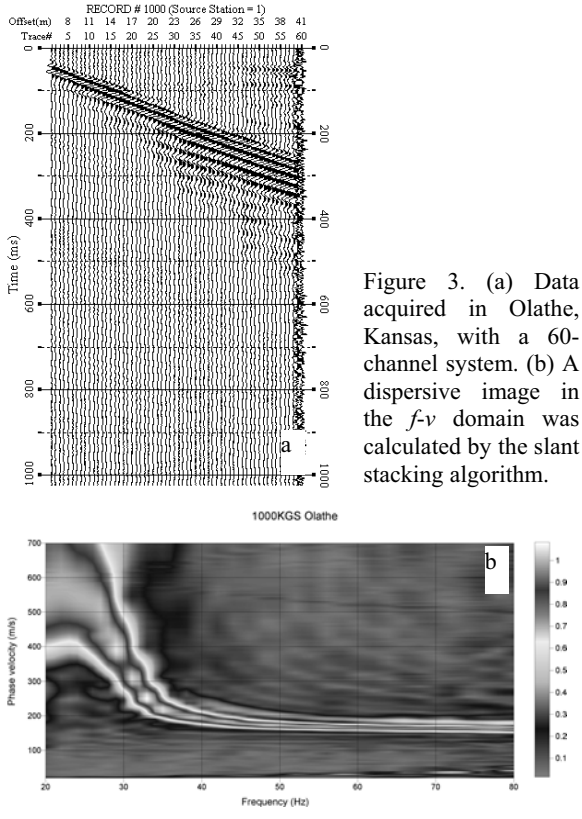

Figure 3. (a) Data acquired in Olathe, Kansas, with a 60-channel system. (b) A dispersive image in the *f-v* domain was calculated by the slant stacking algorithm.

EDITED REFERENCES

Note: This reference list is a copy-edited version of the reference list submitted by the author. Reference lists for the 2005 SEG Technical Program Expanded Abstracts have been copy edited so that references provided with the online metadata for each paper will achieve a high degree of linking to cited sources that appear on the Web.

Imaging dispersive energy by slant stacking

References

Beaty, K. S., D. R. Schmitt, and M. Sacchi, 2002, Simulated annealing inversion of multimode Rayleigh wave dispersion curves for geological structure: Geophysical Journal International, **151**, 622–631.

Beaty, K. S., and D. R. Schmitt, 2003, Repeatability of multimode Rayleigh-wave dispersion studies: Geophysics, **68**, 782–790.

Claerbout, J. F., 1978, Snell waves: Stanford Exploration Project Report No. 15, 57–72.

Coruh, C., 1985, Stretched automatic amplitude adjustment of seismic data: Geophysics, **50**, 252–256.

Goupillaud, P., 1976, Signal design in the "VIBROSEIS" technique: Geophysics, **41**, 1291–1304.

Lin, C. -P., and T. –S. Chang, 2004, Multi-station analysis of surface wave dispersion: Soil Dynamics and Earthquake Engineering, **24**, 877–886.

McMechan, G. A., and M. J. Yedlin, 1981, Analysis of dispersive waves by wave field transformation: Geophysics, **46**, 869–874.

Miller, R. D., J. Xia, C. B. Park, and J. Ivanov, 1999, Multichannel analysis of surface waves to map bedrock: The Leading Edge, **18**, 1392–1396.

Moro, G. D., M. Pipan, E. Forte, and I. Finetti, 2003, Determination of Rayleigh wave dispersion curves for near surface applications in unconsolidated sediments: 73rd Annual International Meeting, Expanded Abstracts, SEG, 1247–1250.

Park, C. B., R. D. Miller, and J. Xia, 1998, Imaging dispersion curves of surface waves on multi-channel record: 68th International Annual Meeting, Expanded Abstracts, SEG, 1377–1380.

Park, C. B., R. D. Miller, and J. Xia, 1999, Multichannel analysis of surface waves: Geophysics, **64**, 800–808.

Schwab, F. A., and L. Knopoff, 1972, Fast surface wave and free mode computations, in B.A. Bolt, eds., Methods in computational physics: Academic Press.

Tian, G., D. W. Steeples, J. Xia, R. D. Miller, K. T. Spikes, and M. D. Ralston, 2003, Multichannel analysis of surface wave method with the autojuggie: Soil Dynamics and Earthquake Engineering, **23**, 243–247.

Tian, G., D. W. Steeples, J. Xia, and K. T. Spikes, 2003, Useful resorting in surface wave method with the autojuggie: Geophysics, **68**, 1906–1908.

Xia, J., C. Chen, P. H. Li, and M. J. Lewis, 2004, Delineation of a collapse feature in a noisy environment using a multichannel surface wave technique: Geotechnique, **54**, 17–27.

Xia, J., R. D. Miller, and C. B. Park, 1999, Estimation of near-surface shear-wave velocity by inversion of Rayleigh wave: Geophysics, **64**, 691–700.

Xia, J., R. D. Miller, C. B. Park, J. A. Hunter, J. B. Harris, and J. Ivanov, 2002, Comparing shear-wave velocity profiles from multichannel analysis of surface wave with borehole measurements: Soil Dynamics and Earthquake Engineering, **22**, 181–190.

Xia, J., R. D. Miller, C. B. Park, and G. Tian, 2002, Determining Q of near-surface materials from Rayleigh waves: Journal of Applied Geophysics, **51**, 121–129.

Xia, J., R. D. Miller, C. B. Park, and G. Tian, 2003, Inversion of high frequency surface waves with fundamental and higher modes: Journal of Applied Geophysics, **52**, 45–57.

Xia, J., R. D. Miller, C. B. Park, E. Wightman, and R. Nigbor, 2002, A pitfall in shallow shear-wave refraction surveying: Journal of Applied Geophysics, **51**, 1–9.

Yilmaz, Ö., 1987, Seismic data processing: SEG.

Yilmaz, Ö., and M. Eser, 2002, A unified workflow for engineering seismology: 72nd Annual International Meeting, SEG, Expanded Abstracts, 1496–1499.